Joint Reconstruction and Segmentation of Real 3D Data in Computed Tomography thanks to a Gauss-Markov-Potts Prior Model,

Camille Chapdelaine, Ali Mohammad-Djafari, Nicolas Gac, Estelle Parra-Denis

Joint Reconstruction and Segmentation of Real 3D Data in Computed Tomography thanks to a Gauss-Markov-Potts Prior Model

Camille Chapdelaine[1,2], Ali Mohammad-Djafari[1], Nicolas Gac[1] and Estelle Parra[2].

[1] Laboratoire des signaux et systèmes, CNRS, Centralesupélec-Univ Paris Saclay, Gif-sur-Yvette, France

[2] SAFRAN SA, Safran Tech, Pôle Technologie du Signal et de l'Information, Magny-Les-Hameaux, France.

***Abstract*— Computed Tomography is a powerful tool to reconstruct a volume in 3D and has a wide field of applications in industry for non-destructive testing. In these applications, the reconstruction process has a key importance to retrieve volumes that can be easily analyzed during the control. In this paper, in order to improve the reconstruction quality, we present a Gauss-Markov-Potts prior model for the object to reconstruct in a Bayesian framework. This model leads to a joint reconstruction and segmentation algorithm which is briefly described. The core of the paper is the application of the algorithm on real 3D data. We show that our method obtains better results than other state-of-art methods. We also propose reconstruction quality indicators without reference which uses both reconstruction and segmentation returned by the algorithm.**

***Index terms*—** 3D Computed Tomography, non-destructive testing, iterative reconstruction algorithm, joint reconstruction and segmentation, Gauss-Markov-Potts

1 Introduction

Computed tomography (CT) is widely used in industry for non-destructive testing (NDT). In many applications, X-rays are projected on a plan of detectors which measure the decrease of their intensity implied by their passing through the industrial part to be controlled. By rotating the object, a set of images is acquired during the acquisition process. Then, these images feed a reconstruction algorithm to retrieve the interior of the object, which make the user able to see if there is any default.

In industry, analytical reconstruction methods, based on Radon transform [1, 2], are widely applied because of they are fast, the most popular of which is FDK algorithm [3]. But these methods suffer from many drawbacks, like artefacts, which require post-reconstruction corrections [4]. Moreover, they have a lack of flexibility when one wants to introduce prior knowledge in order to improve the quality of the reconstruction [5]. On the opposite, algebraic reconstruction techniques (ART) give the possibility to easily take into account this prior knowledge by adding a regularization term to the data matching term. By this way, while the first developed ART, like SIRT [6] or SART [7], simply try to match the data, many recent advanced ART try to find a tradeoff between matching the data and minimization of, for instance, total variation [8] or l_0-norm [9] of the volume to reconstruct. In order to work well and to find the best tradeoff, the most performing methods require to fit parameters, which can be very tedious because the influence of each of these parameters on the result is not always fully understandable. To overcome this difficulty, Bayesian framework is a good way to simultaneously introduce prior information in the reconstruction algorithm and define parameters of which the fitting is simple thanks to their very clear role.

In this framework, we have chosen to develop a Bayesian reconstruction method for NDT in industry using a Gauss-Markov-Potts (GMP) prior model, which has been successfully applied in microwave imaging [10] and image restoration [11]. Thanks to this model, our algorithm is able to reconstruct an industrial part containing several compact regions corresponding to different materials. The innovation of our method is that the segmentation jointly retrieved by our method with the reconstruction can be useful to see defects in the controlled object. In this paper, after having briefly presented the models, we present the results of our method on real 3D phantom, and we compare it to a standard FDK reconstruction and Total Variation (TV) regularization. The goal of this paper is to show the actual efficiency of using Gauss-Markov-Potts prior model on real 3D data : the reconstruction obtained by our method has more constrasted regions than FDK and TV. In [12], the details of the algorithm and some discussion about the choice of the estimators can be found.

2 Prior models

2.1 Forward model

We denote by $\boldsymbol{g}$ the projections, and by $\boldsymbol{f}$ the object to be reconstructed. The linearized discretized forward model for the projections accounting for the noise is :

$$\boldsymbol{g} = \boldsymbol{H}\boldsymbol{f} + \boldsymbol{\epsilon} \tag{1}$$

with

$$\epsilon_i \sim \mathcal{N}(0, v_{\epsilon_i}), \forall i \in \{1, \dots, M\}\,. \tag{2}$$

The variances v_{ϵ_i} are unknowns and are modeled as following an Inverse-Gamma distribution

$$v_{\epsilon_i} \sim \mathcal{IG}(\alpha_{\epsilon_0}, \beta_{\epsilon_0}), \forall i \in \{1, \dots, M\} \tag{3}$$

where α_{ϵ_0} and β_{ϵ_0} are fixed parameters.

2.2 Gauss-Markov-Potts prior model

We now present the model for the controlled object $\boldsymbol{f}$ itself. This object is composed of several materials mapped in several compact and more or less homogeneous regions. We label each voxel j depending on the material to which the voxel belongs. This leads to introduce a hidden discrete field define by : $z_j = k$ if voxel j composes material k, $k \in \{1, \dots, K\}$, with K the total number of materials. The material, or label or class, z_j of a voxel depends on the ones of its neighbours $i \in \mathcal{V}(j)$: that is why we assign markovian model for $\boldsymbol{z}$, which is a Potts model

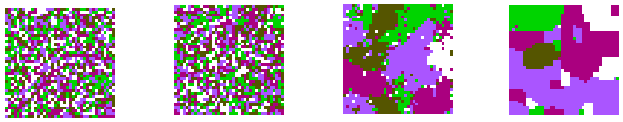

$\gamma_0 = 0.5$ $\gamma_0 = 0.7$ $\gamma_0 = 0.8$ $\gamma_0 = 1.6$

Figure 1: Potts field for different values of γ_0

:

$$p(\boldsymbol{z}|\gamma_0, \boldsymbol{\alpha}) \propto \exp\left[\sum_{j=1}^{N}\left(\sum_{k=1}^{K}\alpha_k\delta(z_j-k)+\gamma_0\sum_{i\in\mathcal{V}(j)}\delta(z_j-z_i)\right)\right] \tag{4}$$

where $\boldsymbol{\alpha}$ and γ_0 are fixed parameters. Potts coefficient γ_0 fits the compacity of the regions. There exits a critical value γ_c above which regions are compact, as illustrated in figure 1. This critical value has been exactly computed in 2D for Ising field ($K = 2$) [13]. Given its label $z_j = k$, voxel j has a gray level f_j distributed around a mean m_k with a variance v_k

$$f_j \sim \mathcal{N}(m_k, v_k) \text{ if } z_j = k. \tag{5}$$

The means $\boldsymbol{m}$ and variances $\boldsymbol{v}$ of the classes are unknown and have the following priors

$$m_k \sim \mathcal{N}(m_0, v_0), \forall k \in \{1, \ldots, K\} \tag{6}$$

and

$$v_k \sim \mathcal{IG}(\alpha_0, \beta_0), \forall k \in \{1, \ldots, K\} \tag{7}$$

where m_0, v_0, α_0 and β_0 are fixed parameters.

3 Joint Maximization A Posteriori (JMAP) algorithm

After having built our prior models, the reconstruction algorithm consists in estimating each unknown $\boldsymbol{f}, \boldsymbol{z}, \boldsymbol{v}_\epsilon, \boldsymbol{m}$ and $\boldsymbol{v}$ by maximizing their joint posterior probability

$$(\hat{\boldsymbol{f}}, \hat{\boldsymbol{z}}, \hat{\boldsymbol{v}}_\epsilon, \hat{\boldsymbol{m}}, \hat{\boldsymbol{v}}) = \underset{(\boldsymbol{f},\boldsymbol{z},\boldsymbol{v}_\epsilon,\boldsymbol{m},\boldsymbol{v})}{\arg\max} \{p(\boldsymbol{f}, \boldsymbol{z}, \boldsymbol{v}_\epsilon, \boldsymbol{m}, \boldsymbol{v}|\boldsymbol{g}; \mathcal{M})\} \tag{8}$$

thanks to the approximate maximization iterative algorithm

$$\begin{cases} \boldsymbol{f}^{(t)} \leftarrow \arg\max_{\boldsymbol{f}} \left\{p(\boldsymbol{f}, \boldsymbol{z}^{(t-1)}, \boldsymbol{v}_\epsilon^{(t-1)}, \boldsymbol{m}^{(t-1)}, \boldsymbol{v}^{(t-1)}|\boldsymbol{g}; \mathcal{M})\right\} \\ \boldsymbol{z}^{(t)} \leftarrow \arg\max_{\boldsymbol{z}} \left\{p(\boldsymbol{f}^{(t)}, \boldsymbol{z}, \boldsymbol{v}_\epsilon^{(t-1)}, \boldsymbol{m}^{(t-1)}, \boldsymbol{v}^{(t-1)}|\boldsymbol{g}; \mathcal{M})\right\} \\ \boldsymbol{v}_\epsilon^{(t)} \leftarrow \arg\max_{\boldsymbol{v}_\epsilon} \left\{p(\boldsymbol{f}^{(t)}, \boldsymbol{z}^{(t)}, \boldsymbol{v}_\epsilon, \boldsymbol{m}^{(t-1)}, \boldsymbol{v}^{(t-1)}|\boldsymbol{g}; \mathcal{M})\right\} \\ \boldsymbol{m}^{(t)} \leftarrow \arg\max_{\boldsymbol{m}} \left\{p(\boldsymbol{f}^{(t)}, \boldsymbol{z}^{(t)}, \boldsymbol{v}_\epsilon^{(t)}, \boldsymbol{m}, \boldsymbol{v}^{(t-1)}|\boldsymbol{g}; \mathcal{M})\right\} \\ \boldsymbol{v}^{(t)} \leftarrow \arg\max_{\boldsymbol{v}} \left\{p(\boldsymbol{f}^{(t)}, \boldsymbol{z}^{(t)}, \boldsymbol{v}_\epsilon^{(t)}, \boldsymbol{m}^{(t)}, \boldsymbol{v}|\boldsymbol{g}; \mathcal{M})\right\} \end{cases} \tag{9}$$

where index t denotes the iteration t. This algorithm is a type of variational bayesian approximation [14] which is a local optimization. By applying Bayes rule

$$\begin{aligned} p(\boldsymbol{f}, \boldsymbol{z}, \boldsymbol{v}_\epsilon, \boldsymbol{m}, \boldsymbol{v}|\boldsymbol{g}; \mathcal{M}) \quad &\propto p(\boldsymbol{g}|\boldsymbol{f}, \boldsymbol{v}_\epsilon)\, p(\boldsymbol{f}|\boldsymbol{z}, \boldsymbol{m}, \boldsymbol{v}) \\ &\quad p(\boldsymbol{v}_\epsilon|\alpha_{\epsilon_0}, \beta_{\epsilon_0})\, p(\boldsymbol{z}|\boldsymbol{\alpha}; \gamma_0) \\ &\quad p(\boldsymbol{m}|m_0, v_0)\, p(\boldsymbol{v}|\alpha_0, \beta_0), \end{aligned} \tag{10}$$

each step of the algorithm can be performed, as we have detailed in [12]. Thanks to this method, we see that an estimation of the object $\boldsymbol{f}$ and the labels $\boldsymbol{z}$, i.e. a segmentation of the object, are retrieved. This is a great advantage, because there is only one source of uncertainties in the control process, while, when applying many other methods, the reconstruction algorithm and the post-reconstruction segmentation algorithm are two different sources of uncertainties.

4 Results on real 3D IQI data

The considered volume is a real 3D IQI phantom [15], discretized in $512 \times 512 \times 256$ voxels. The data are 300 projections of size 512×512 pixels. The number of materials in the volume to reconstruct is $K = 4$. We apply our method and compare it with FDK [3] and Total Variation (TV) minimization reconstruction methods. Concerning TV, it is implemented by following the algorithm proposed in [16], based on Bregman iteration [17].

4.1 Initialization

To apply JMAP algorithm described in section 3, an initial volume and an initial segmentation are required. As initial volume, because we have many projections, we use FDK reconstruction, shown in figure 2. Next, we need a segmentation of this initial volume as initial segmentation. This segmentation is obtained by a non-uniform thresholding of FDK reconstruction.

To determine the thresholds, we estimate the histogram of the initial volume. Then, we apply the peak-picking algorithm explained in [18] and originally developped for non-parametric clustering [19]. For each bin, we seek the nearest peak in its neighbourhood : this peak is called the parent-bin of the current bin, which is so called a child-bin of this peak. Each parent-bin and its children are seen as a class, i.e. the voxels in the children-bins of parent-bin k are assigned the initial class k. Because we know the number of classes ($K = 4$), each parent-bin is assigned as the child-bin of a higher parent-bin in its neighbourhood until there are only $K = 4$ parents-bins. This gives the segmentation shown in figure 3, used as initial segmentation by JMAP algorithm.

4.2 Results and comparison with FDK

Table 1 summarizes the values of most of the parameters we fixed to perform the joint reconstruction and segmentation of IQI data. The controlled volume is composed of 3 materials and air : that is why we fix $K = 4$. The other parameters are fixed according to a strategy we propose in [12]. Thanks to the clear Bayesian prior model, tuning the parameters of JMAP is straightforward, while it is more tedious for TV.

Parameters	α_{ϵ_0}	K	γ_0	v_0	α_0	β_0
Fixed values	2.1	4	3	1	5	0.01

Table 1: Reconstruction parameters for 3D IQI data

Next, we run JMAP algorithm and we obtain the reconstruction and the segmentation shown in figures 6 and 7 respectively. When comparing FDK, TV and JMAP reconstructions in figures 2, 4 and 6 respectively, we can see the external circle surrounding the object in FDK reconstruction is completely erased by JMAP algorithm. Moreover, the JMAP reconstruction is more constrasted than the FDK and TV reconstructions, especially for the white region in the top of the object. This better contrast is still emphasized when in figure 8, we plot the profiles of the little holes in the bottom of the object : the profile of JMAP reconstruction is sharper than the one of FDK reconstruction.

To deepen the comparison, we have defined three reconstruction quality indicators. The first focuses on the compactness of

the classes and is defined as :

$$C_{omp} = \frac{1}{K}\sum_{k=1}^{K}\frac{1}{N_k}\sum_{j\in\mathcal{R}_k}\frac{1}{N_{\mathcal{V}}}\sum_{i\in\mathcal{V}(j)}\delta(k-z_i) \tag{11}$$

where $\mathcal{R}_k = \{j|z_j = k\}$. The second measures the distinguishability of the classes on the contours :

$$d_{ist} = 1 - \frac{1}{K}\sum_{k=1}^{K}\frac{1}{N_k}\sum_{j\in\mathcal{R}_k}(\hat{d}_{ist})_j \tag{12}$$

with, if $z_j = k$:

$$(\hat{d}_{ist})_j = \begin{cases} \frac{\sum_{i\in\mathcal{V}(j)}\exp\left(-(f_j-f_i)^2\right)(1-\delta(k-z_i))}{\sum_{i\in\mathcal{V}(j)}(1-\delta(k-z_i))} & \text{if } j \text{ is on a contour} \\ 0 \text{ otherwise} \end{cases} \tag{13}$$

The third indicator which quantifies how homogeneous the classes are :

$$h_{omo} = \frac{1}{K}\sum_{k=1}^{K}\frac{1}{N_k}\sum_{j\in\mathcal{R}_k}(\hat{h}_{omo})_j \tag{14}$$

with, if $z_j = k$:

$$(\hat{h}_{omo})_j = \frac{\sum_{i\in\mathcal{V}(j)}\exp\left(-(f_j-f_i)^2\right)\delta(k-z_i)}{\sum_{i\in\mathcal{V}(j)}\delta(k-z_i)} \tag{15}$$

if $\sum_{i\in\mathcal{V}(j)}\delta(k-z_i) \neq 0$. Otherwise, $(\hat{h}_{omo})_j = 0$.

In this way, we have three reconstruction quality indicators which respectively measure compactness, distinguishability and homogeneity of the classes in the reconstruction. These indicators are designed such that the higher they are, the better the reconstruction is. One shall notice they need a segmentation of the reconstruction to be applied. In table 2, we compute them on the joint recontruction and segmentation retrieved by JMAP, on the initial reconstruction by FDK in figure 2 and the initial segmentation of this reconstruction in figure 3, and on TV reconstruction and its posterior segmentation in figure 5, obtained thanks to a Gauss-Markov-Potts prior model proposed in [20]. Because the labels of each of the three reconstruction are very similar, C_{omp} is almost the same for the three methods. Concerning d_{ist} and h_{omo} achieves the highest values, which confirms that our method outperform FDK and TV.

Indicator	C_{omp}	d_{ist}	h_{omo}
FDK	94.4 %	78.4 %	78.3 %
TV	94.5 %	77.5 %	77.5 %
JMAP	94.3 %	79.0 %	78.8 %

Table 2: Comparison of FDK, TV and JMAP using reconstruction quality indicators

5 Conclusion and perspectives

In this paper, we have presented results on real 3D phantom of a reconstruction method which has achieved high compactness, distinguishability and homogeneity of the classes obtained by the segmentation performed jointly with the reconstruction. Thanks to clear prior models, the parameters of the algorithm have been proved easy to fit. The method has shown better results than both FDK and TV reconstructions. An important future work would be to propose a massively parallelized version of the algorithm on GPU.

References

[1] K. T. Smith and F. Keinert, "Mathematical foundations of computed tomography," *Applied Optics*, vol. 24, no. 23, pp. 3950–3957, 1985.

[2] T. Rodet, *Algorithmes rapides de reconstruction en tomographie par compression des calculs: application à la tomofluoroscopie 3D*. PhD thesis, Grenoble, INPG, 2002.

[3] L. Feldkamp, L. Davis, and J. Kress, "Practical cone-beam algorithm," *JOSA A*, vol. 1, no. 6, pp. 612–619, 1984.

[4] M. Krumm, S. Kasperl, and M. Franz, "Reducing non-linear artifacts of multi-material objects in industrial 3d computed tomography," *Ndt & E International*, vol. 41, no. 4, pp. 242–251, 2008.

[5] A. Mohammad-Djafari and G. Demoment, "Maximum entropy image reconstruction in X-ray and diffraction tomography," *Medical Imaging, IEEE Transactions on*, vol. 7, no. 4, pp. 345–354, 1988.

[6] P. Gilbert, "Iterative methods for the three-dimensional reconstruction of an object from projections," *Journal of theoretical biology*, vol. 36, no. 1, pp. 105–117, 1972.

[7] A. H. Andersen and A. C. Kak, "Simultaneous algebraic reconstruction technique (SART): a superior implementation of the ART algorithm," *Ultrasonic imaging*, vol. 6, no. 1, pp. 81–94, 1984.

[8] E. Y. Sidky, H. Jakob, X. Pan, *et al.*, "Convex optimization problem prototyping for image reconstruction in computed tomography with the Chambolle & Pock algorithm," *Physics in medicine and biology*, vol. 57, no. 10, p. 3065, 2012.

[9] M. Storath, A. Weinmann, J. Frikel, and M. Unser, "Joint image reconstruction and segmentation using the Potts model," *Inverse Problems*, vol. 31, no. 2, p. 025003, 2015.

[10] O. Féron, B. Duchêne, and A. Mohammad-Djafari, "Microwave imaging of inhomogeneous objects made of a finite number of dielectric and conductive materials from experimental data," *Inverse Problems*, vol. 21, no. 6, p. S95, 2005.

[11] H. Ayasso and A. Mohammad-Djafari, "Joint NDT image restoration and segmentation using Gauss–Markov–Potts prior models and variational bayesian computation," *Image Processing, IEEE Transactions on*, vol. 19, no. 9, pp. 2265–2277, 2010.

[12] C. Chapdelaine, A. Mohammad-Djafari, N. Gac, and E. Parra, "A 3D Bayesian Computed Tomography Reconstruction Algorithm with Gauss-Markov-Potts Prior Model and its Application to Real Data," *Fundamenta Informaticae*, submitted.

[13] J.-F. Giovannelli, "Estimation of the Ising field parameter thanks to the exact partition function," in *ICIP*, pp. 1441–1444, 2010.

[14] A. Mohammad-Djafari and H. Ayasso, "Variational Bayes and mean field approximations for Markov field unsupervised estimation," in *2009 IEEE International Workshop on Machine Learning for Signal Processing*, pp. 1–6, IEEE, 2009.

[15] L. Gay, P. Arslan, Y. Rambourg, and A. Chandelle, "Fantôme destiné à être utilisé pour le contrôle de la qualité d'images tomographiques," June 2016.

[16] T. Goldstein and S. Osher, "The split Bregman method for L1-regularized problems," *SIAM journal on imaging sciences*, vol. 2, no. 2, pp. 323–343, 2009.

[17] L. M. Bregman, "The relaxation method of finding the common point of convex sets and its application to the solution of problems in convex programming," *USSR computational mathematics and mathematical physics*, vol. 7, no. 3, pp. 200–217, 1967.

[18] F. Kurugollu, B. Sankur, and A. E. Harmanci, "Color image segmentation using histogram multithresholding and fusion," *Image and vision computing*, vol. 19, no. 13, pp. 915–928, 2001.

[19] W. L. G. Koontz, P. M. Narendra, and K. Fukunaga, "A graph-theoretic approach to nonparametric cluster analysis," *IEEE Transactions on Computers*, vol. 100, no. 9, pp. 936–944, 1976.

[20] R.-G. Rosu, J.-F. Giovannelli, A. Giremus, and C. Vacar, "Potts model parameter estimation in Bayesian segmentation of piecewise constant images," in *2015 IEEE International Conference on Acoustics, Speech and Signal Processing (ICASSP)*, pp. 4080–4084, IEEE, 2015.

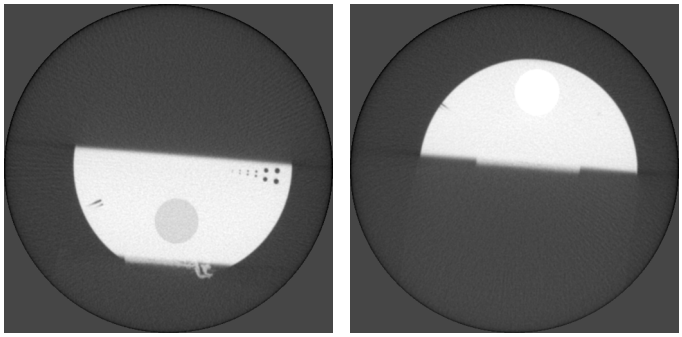

Figure 2: FDK reconstruction (bottom and top)

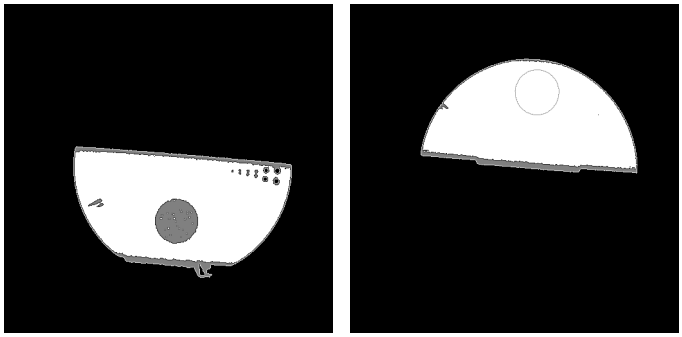

Figure 3: Segmentation of FDK reconstruction (bottom and top)

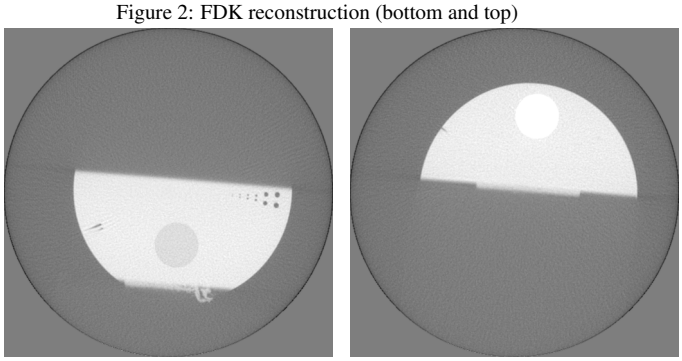

Figure 4: Reconstruction obtained by TV (bottom and top)

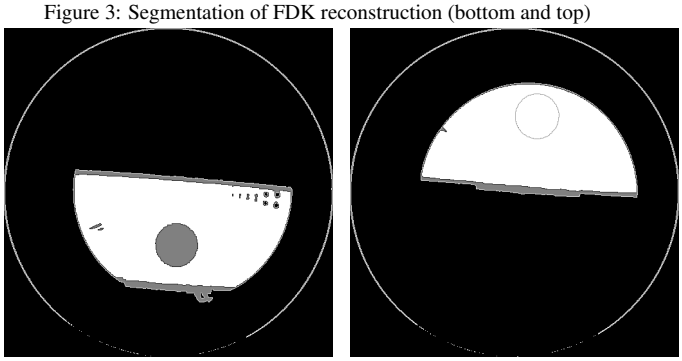

Figure 5: Segmentation of TV reconstruction (bottom and top)

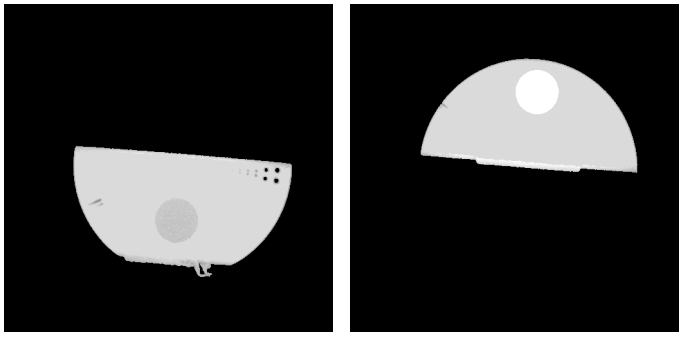

Figure 6: Reconstruction obtained by JMAP (bottom and top)

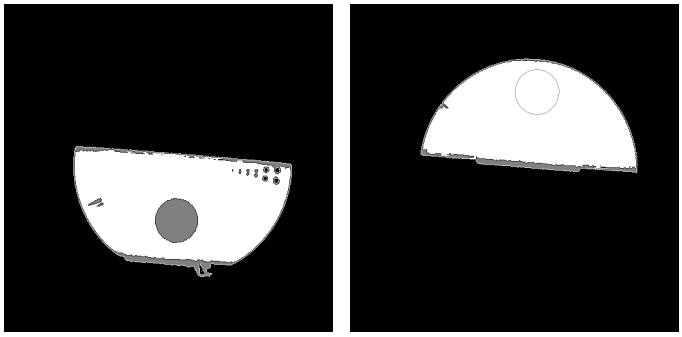

Figure 7: Segmentation obtained by JMAP (bottom and top)

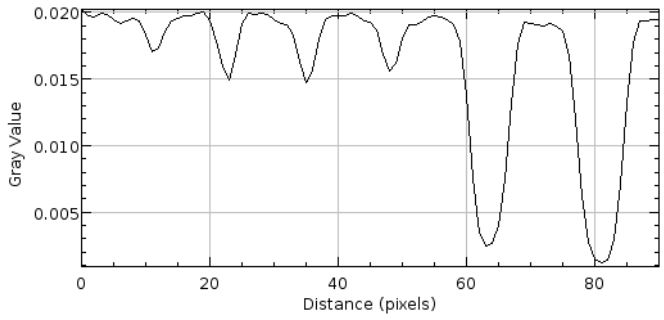

(a)

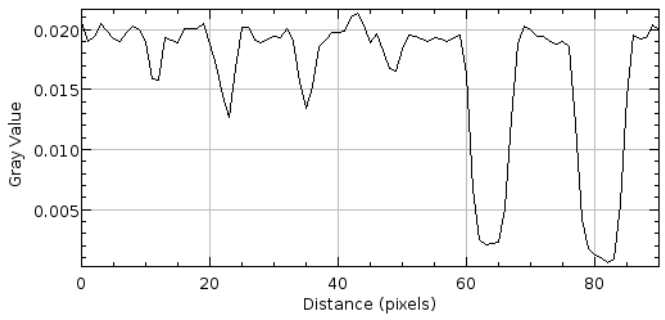

(b)

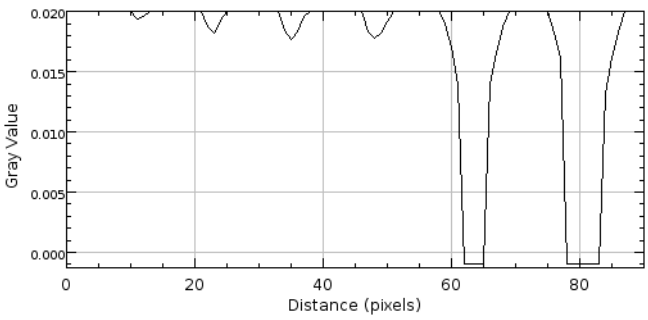

(c)

Figure 8: Profiles of holes for FDK (a), TV (b) and JMAP (c) reconstructions